Persistent Luminescence Nanoparticles for Bioimaging

Cyrille Richard, Thomas Maldiney, Quentin Le Masne de Chermont, Johanne Seguin, Nicolas Wattier, Gabriel Courties, Florence Apparailly, Michel Bessodes, Daniel Scherman

Persistent Luminescence Nanoparticles for Bioimaging

Cyrille Richard, Thomas Maldiney, Quentin le Masne de Chermont, Johanne Seguin, Nicolas Wattier, Gabriel Courties, Florence Apparailly, Michel Bessodes, and Daniel Scherman

Abstract : Optical imaging is a rapidly developing field of research aimed at non-invasive monitoring of disease progression, evaluating the effects and pharmacokinetic of a drug, or identifying pathological biomarkers. To this end, it requires the development of targeting and highly specific contrast agents. In fluorescence imaging, an external light of appropriate wavelength is used to excite the fluorescent molecule, followed almost immediately by the release of longer wavelength, lower energy light for imaging. Fluorescence is increasingly used for imaging and has provided remarkable results. However this technique presents several limitations, especially due to tissue autofluorescence under external illumination and weak tissue penetration of low wavelength excitation light. To overcome these drawbacks, we have developed an innovative technique using persistent luminescence nanoparticles (PLNP) for optical imaging in small animal. Such nanoparticles can be excited before systemic injection, and their biodistribution monitored in real-time for dozen of minutes without the need for any external illumination source. This review article will focus on recent works undertaken in our laboratory on the synthesis of PLNP, their surface modifications and applications for bioimaging.

Key words: Nanoparticle; Persistent luminescence; Silicate; Surface coating; Biodistribution; Tumor targeting; Inflammation; Biomedical imaging

---

Cyrille Richard, Thomas Maldiney, Quentin le Masne de Chermont, Johanne Seguin, Nicolas Wattier, Michel Bessodes, Daniel Scherman
Unité de Pharmacologie Chimique et Génétique et d'Imagerie; CNRS, UMR 8151, Paris, F-75270 cedex France; Inserm, U1022, Paris, F-75270 cedex France; Université Paris Descartes, Faculté des Sciences Pharmaceutiques et Biologiques, Paris, F-75270 cedex France; ENSCP, Chimie Paristech, Paris, F-75231 cedex France. e-mail: daniel.scherman@univ-paris5.fr

Gabriel Courties, Florence Apparailly
Inserm, U844, Montpellier, F-34091 France; Université Montpellier 1, UFR de Médecine, Montpellier, F-34000 France ; Service d'immuno-rhumatologie, Hôpital Lapeyronie, Montpellier, F-34295 France.

1 Introduction

From fluorescent organic dyes to luminescent nanocrystals, optical imaging raises growing interest for the understanding of physiological mechanisms or the development of new diagnosis and therapeutic applications [Weissleder et al. 2008]. Photonic probes offer not only practicable living sensors, but also rely on low-cost or affordable imaging devices and techniques. The semiconductor Quantum Dots (QDs) [Medintz et al. 2005][Smith et al. 2008] exhibit high quantum yield, good photostability and tunable emission wavelength. Luminescent porous silicon nanoparticles can act as both diagnostic [Li et al. 2004] and therapeutic tools [Salonen et al. 2007]. At last, near-infrared fluorescent molecules [Chen et al. 2005] offer the possiblity to work with very low autofluorescence from tissues under constant illumination.

Each of the above-mentioned probes displays characteristics that limit preclinical use or future therapeutic application. First, the emission wavelength of semiconductor QDs must be tuned by changing the particle diameter (ranging from 2 nm to 10 nm) or its composition. On the one hand, this opens alternatives for renal clearance [Choi 2007], but on the other hand it also shortens circulation time of the probe and impairs effective targeting, levying strict regulations on its design [Longmire et al. 2008]. Luminescent porous silicon nanoparticles show great promise as non-toxic, self-destructive, and traceable cargo for anti-cancer drugs, but they suffer from limited quantum yield [Park et al. 2009] ($\sim 10\%$) compared to QDs ($> 80\%$ in organic solvent). As for near-infrared fluorescent probes, it is now well established that organic dyes are susceptible to photobleaching, and are most often unstable under physiological conditions, which make them hardly the best candidate for a long-term biological or biomedical purpose [Resch-Genger et al. 2008].

To overcome these difficulties, we have recently developed persistent luminescence silicate nanoparticles [le Masne de Chermont et al. 2007], referred to as PLNP, suitable for in vivo imaging, and specially designed to avoid most inherent problems encountered in classical optical systems. The key element of this technology is based on a new generation of long-luminescence nanoparticles, emitting in the near-infrared region, that can be optically excited before in vivo local or systemic injection. This long-lasting afterglow prevents residual background noise originating from in situ excitation and can last several hours. Thus, the significant signal-to-noise ratio improvement allows detection in rather deep organs and real-time biodistribution monitoring of active elements hours after injection.

2 Persistent luminescence nanoparticles from silicate host

Great progress have been made in long-lasting phosphorescence since the early 20th century. Long-lasting phosphors were widely used in emergency lighting, safety in-

dications, road signs and so on. Most of the long-lasting phosphors are based on sulfides and aluminates. Recently silicate phosphors have been paid considerable attention because of their bright phosphorescence, notably in blue and green regions [Jiang et al. 2003]. In 2003, Wang et al. reported the synthesis of $MgSiO_3$ enstatite, doped with Eu^{2+}, Dy^{3+} and Mn^{2+} luminescent ions, showing a long red persistent luminescence [Wang et al. 2003]. This article initiated in our laboratory the preparation of several luminescent silicates intended for bioimaging applications.

2.1 Synthesis of enstatite-like silicates: $MgSiO_3$, $ZnMgSi_2O_6$ and $Ca_{0.2}Zn_{0.9}Mg_{0.9}Si_2O_6$ doped with Eu^{2+}, Dy^{3+} and Mn^{2+}

2.1.1 The sol-gel process

Persistent luminescence materials are generally synthesized by a solid-state reaction, giving micrometer-sized particles. Such large particles would hardly circulate after systemic injection to small animals, thus limiting bioimaging applications. For this reason, we preferred a Sol-Gel approach to synthesize smaller particles [Brinker et al. 1990]. Raw materials used in our routine synthesis are: magnesium nitrate ($Mg(NO_3)_2$, $6H_2O$), zinc chloride ($ZnCl_2$), calcium chloride ($CaCl_2$, $2H_2O$), europium chloride ($EuCl_3$, $6H_2O$), dysprosium nitrate ($Dy(NO_3)_3$, $5H_2O$), manganese chloride ($MnCl_2$, $4H_2O$), and tetraethoxysilane (TEOS). Depending on the desired nanomaterial ($MgSiO_3$, $ZnMgSi_2O_6$ or $Ca_{0.2}Zn_{0.9}Mg_{0.9}Si_2O_6$) different amount of reagents were used [le Masne de Chermont et al. 2009]. For example, for the synthesis of $Ca_{0.2}Zn_{0.9}Mg_{0.9}Si_2O_6$ (where 10% of Zn and Mg atoms were substituted for Ca) doped with 0.5% Eu^{2+}, 1% Dy^{3+}, and 2.5 % Mn^{2+} (the percentages are based on metallic cations content), we used: 125 mg of calcium chloride, 990 mg of magnesium nitrate, 525 mg of zinc chloride, 16 mg of europium chloride, 39 mg of dysprosium nitrate, 44 mg of manganese chloride, 4 mL of deionized water at pH 2 and 2 mL of TEOS. The mixture is vigourously stirred at room temperature for 1 hour and then for 2 hours at 70°C until the sol-gel transition occured. The wet gel was then dried in an oven at 110°C for 20 h to remove water and ethanol (Figure 1).

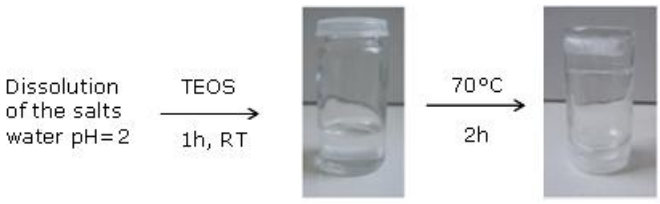

Fig. 1 Hydrolysis of TEOS in the presence of the salts and sol-gel transition. Sol in the middle, gel on the right.

2.1.2 Heating to get crystals

The resulting opaque dry gel is then calcined in a zircone crucible under a weak reductive atmosphere using 10% H_2, 90% Ar (Noxal 4, Air Liquide, Düsseldorf, Germany). Depending on the material we want, the final sintering temperature must be adapted. To prepare $Ca_{0.2}Zn_{0.9}Mg_{0.9}Si_2O_6$ (Eu^{2+}, Dy^{3+}, Mn^{2+}), the gel is fired at 1050°C for 10 h and slowly cooled down to room temperature to give white crystals (Figure 2).

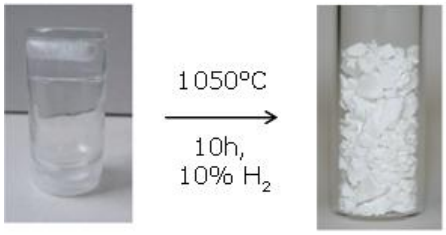

Fig. 2 Heating of the gel to get crystals.

2.2 Characterisation of synthesized nanomaterials

2.2.1 Fluorescence spectra

Optical spectra, shown in Figure 3, were recorded with a Varian (Palo Alto, CA) Cary-Eclipse Fluorescence spectrophotometer by using the phosphorescence mode with a delay and a gate time of 300 ms (for excitation spectrum: em = 690 nm; excitation slit = 5 nm; emission slit = 20 nm) (for excitation spectrum: ex = 340 nm; excitation slit = 20 nm; emission slit = 5 nm). About 50 mg of each powder were deposited on a glass plate, stuck with a few drops of ethanol and inserted into the spectrophotometer.

2.2.2 Luminescence

To record persistent luminescence decline curves, 10 mg of each material were deposited on a 96-wells plate, excited for 2 min with a UV lamp, and placed under the photon-counting system consisting of a cooled GaAs intensified charge-coupled device (ICCD) camera (Photon Imager; Biospace Lab, Paris, France) without any external illumination system. Luminescence intensity was detectable for more than 24 h when kept in the dark. The decay kinetics (Figure 4) were found to be close to a power law $I \approx I_0 \cdot t^{-n}$ (n = 0.96, R^2 = 0.996) after the first 100 s.

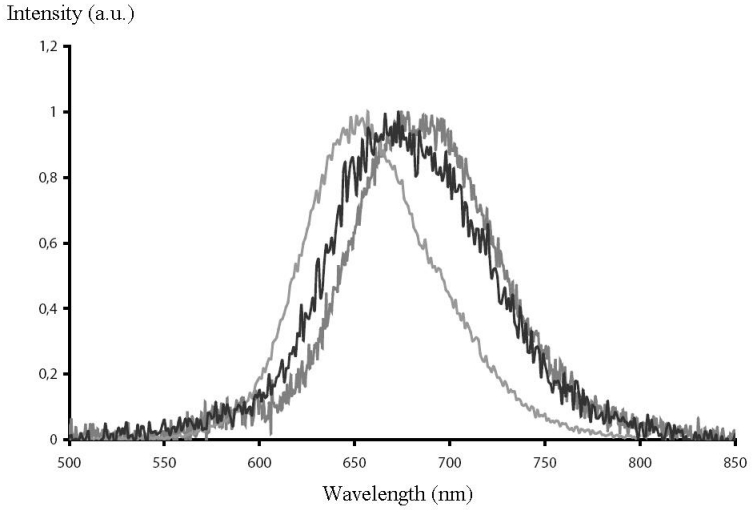

Fig. 3 Emission spectra of the three synthesized materials doped with Eu^{2+}, Dy^{3+}, Mn^{2+}. $MgSiO_3$ (λ_{em} = 645 nm), $ZnMgSi_2O_6$ (λ_{em} = 660 nm), $Ca_{0.2}Zn_{0.9}Mg_{0.9}Si_2O_6$ (λ_{em} = 690 nm).

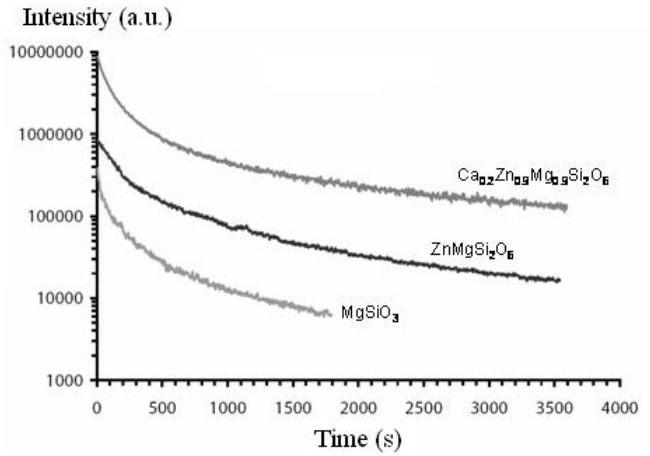

Fig. 4 Afterglow decays after UV excitation of the materials doped with Eu^{2+}, Dy^{3+}, Mn^{2+}. $MgSiO_3$, $ZnMgSi_2O_6$, $Ca_{0.2}Zn_{0.9}Mg_{0.9}Si_2O_6$.

For bioimaging application, we selected the $Ca_{0.2}Zn_{0.9}Mg_{0.9}Si_2O_6$ composition since it had the best characteristics in terms of emission wavelength (690 nm, which is located within the transparency window) and of luminescence intensity (the highest among all three synthesized silicates).

3 Chemical surface functionalization of silicates

3.1 Obtention of nanoparticles of different sizes

Nanometer-sized particles were obtained by basic wet grinding of the solid (500 mg) for 15 minutes with a mortar and pestle in a minimum volume of 5 mM NaOH solution. Hydroxylation was then performed overnight by dispersing the ground powder ($Ca_{0.2}Zn_{0.9}Mg_{0.9}Si_2O_6$ doped with Eu^{2+}, Dy^{3+}, and Mn^{2+}) in 50 mL of the same NaOH solution to get hydroxyl-PLNP. Nanoparticles with a diameter of 180 nm were selected from the whole polydisperse colloidal suspension by centrifugation on a SANYO MSE Mistral 1000 at 4500 rpm for 5 minutes (centrifugation time was lengthened to 30 min in order to obtain 120 nm PLNP). They were located in the supernatant (assessed by Dynamic Light Scattering). The supernatants were gathered and concentrated to a final 5 mg/mL suspension. PLNP with a diameter of 80 nm were selected from the 120 nm concentrated suspension by centrifugation on an Eppendorf MiniSpin Plus at 8000 rpm for 5 minutes. Following a similar approach, centrifugation steps were repeated 4 times and the resulting suspension concentrated to a final amount of 5 mg/mL [Maldiney et al. 2011].

3.2 Characterization of the nanoparticles by DLS and TEM

3.2.1 Dynamic light scattering measurements

Photon correlation spectroscopy is a technique used to determine the diffusion coefficient of small particles in a liquid. The coefficient is determined by accurately measuring the light scattering intensity of the particles as a function of time. Dynamic light scattering (DLS) was performed on a Nano ZS (Malvern Instruments, Southborough, MA) equipped with a 632.8 nm helium neon laser and 5 mW power, with a detection angle at 173° (noninvasive back scattering).

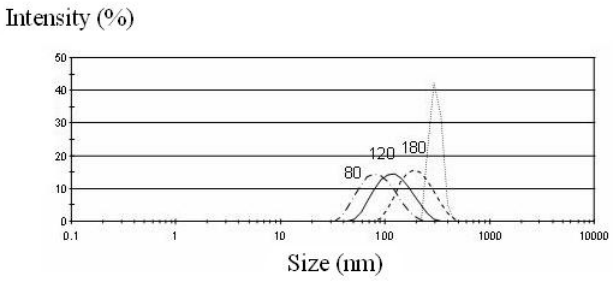

Fig. 5 Size of the different nanoparticles determined by dynamic light scattering.

3.2.2 Transmission electron microscopy

Electronic microscopy analysis was used to show both the shape and size of $Ca_{0.2}Zn_{0.9}Mg_{0.9}Si_2O_6$ nanoparticles doped with luminescent ions (Figure 6).

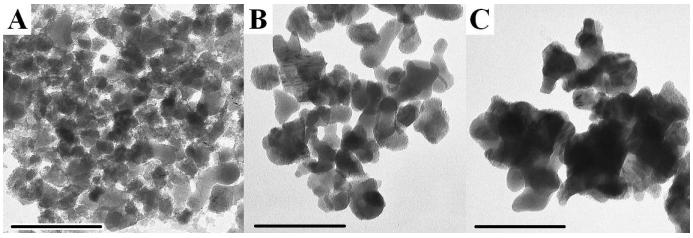

Fig. 6 TEM image of different size $Ca_{0.2}Zn_{0.9}Mg_{0.9}Si_2O_6$: Eu^{2+}, Dy^{3+}, Mn^{2+}. A: 80 nm. B: 120 nm. C: 180 nm. Scale bar = 100 nm. [Maldiney et al. 2011]

3.3 Surface functionalization

In vivo biodistribution of nanoparticles highly depends on their charge and surface properties. Chemical modification of the surface of the probe is critical to better control its circulation and hope for a future targeting to a specific region of interest. For this reason, the PLNP were first reacted with 3-aminopropyl-triethoxysilane (APTES), in order to provide positively charged PLNP (referred to amino-PLNP) resulting from the presence of free amino groups at the surface. The APTES in excess was removed by several sedimentation washing procedures. The global surface charge of the amino-PLNP was reversed by condensation with diglycolic anhydride, which reacted with amines to give free carboxyl groups (carboxy-PLNP). As the use of polyethylene glycol (PEG) capping has already been shown to increase the circulation time of several colloidal systems [Moghimi et al. 2001], we also conducted coupling of different PEG moieties (either 5, 10 or 20 kDa) with the amino-PLNP (Figure 7).

3.4 Characterization of the functionalized PLNP

3.4.1 Zeta potential

The success of the grafting procedure was assessed by zeta potential measurements (Figure 8). The zeta potential of amino-PLNP was positive (+35.8 mV at pH 7),

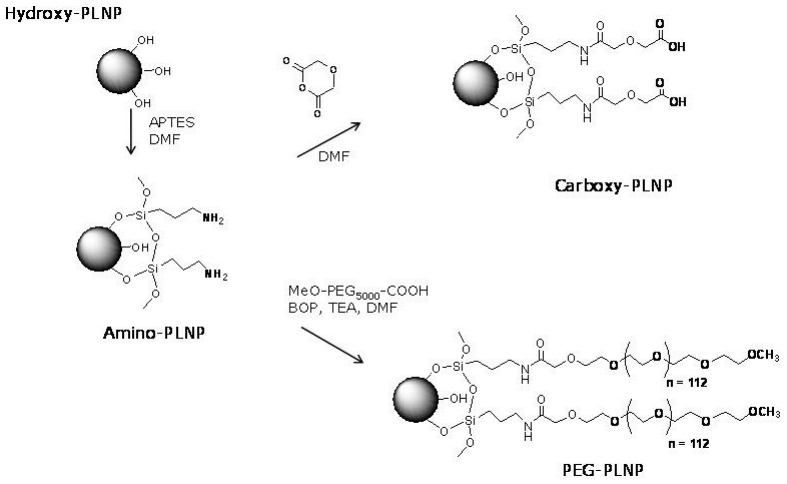

Fig. 7 PLNP surface modification with different molecules.

the zeta potential of carboxyl-PLNP was negative (-50.3 mV at pH 7). Finally as expected, PEGylation of PLNP led to neutral particles (+1 mV).

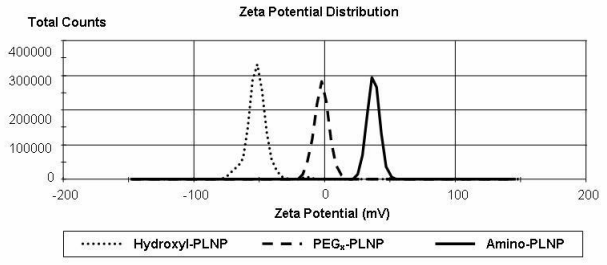

Fig. 8 Zeta potential of PLNP after each surface modification. [Maldiney et al. 2011]

3.4.2 Thermogravimetric analysis

It exists several chemical methods to determine the amount of a given molecule grafted on nanoparticles. They usually rely on the reactivity of known chemical motifs on the ligand to dose, generally amines, carboxyl or carbonyl groups. In the case of PEG coverage, these methods could not be considered since the polymer lacked reactive functions. However, the relative high molecular weight of the chain

opened alternative to a sensitive dosing of PEG moiety through thermogravimetric analysis (TGA). Briefly, TGA analysis was performed by gradually heating the sample from 20°C to 780°C under Argon atmosphere. Precision scales allowed to monitor the weight loss as a function of temperature. Weight loss curves for 120 nm PLNP were recorded after each functionalization step. From amino-PLNP to PEGylated PLNP we clearly distinguish two stages in surface decomposition. First, water trapped in the organic layer on the surface of PLNP evaporates before 325°C. The second stage begins after 325°C and corresponds to the decomposition of organic APTES and PEG coverage on the particles. When comparing TG curves for different PEG, we notice that the longer the PEG chain length, the fewer PEGylated chains remain grafted on the surface. Calculated values from weight loss percentages indicate that in the case of 5 kDa PEG, polymer concentration reaches about 15 nmol/mg of PLNP. This value drops significantly when increasing the size of the PEG to 9 nmol/mg for 10 kDa PEG and 3 nmol/mg for 20 kDa PEG. Despite the 20 fold molar excess of PEG (compared to the amount of free amino groups previously estimated on the surface: about 60 nmol/mg), it seems that steric hindrance hampers the approach of larger PEG near the particle, thus preventing quantitative reaction as well as equimolar loadings of the different PEG.

3.4.3 Colloidal stability

Before any use of these nanoparticles for bioimaging, colloidal stability in biological media had to be checked. As shown in Figure 9, the addition of polyethylene glycol significantly changes the average value of hydrodynamic diameter, leading to particles from 40 to 70 nm larger than the initial hydroxyl-PLNP, and providing high colloidal stability in normal saline solution.

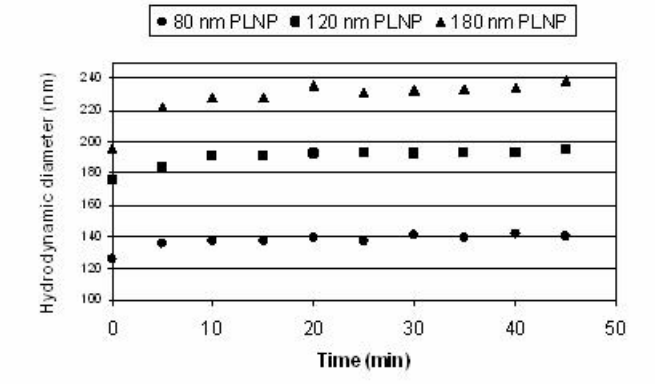

Fig. 9 Colloidal stability of 5 kDa PEG-PLNP: evolution of the hydrodynamic diameter in 150 mM NaCl for 45 minutes. [Maldiney et al. 2011]

4 Bioimaging with persistent luminescence nanoparticles

4.1 Principle

As explained in the introduction, the major difference between our luminescent silicate and other classical optical probes (used for bioimaging) comes from the ability of PLNP to store excitation energy and to emit at higher wavelength from dozen of minutes to hours. This property allows to excite the probe before its systemic injection (Figure 10).

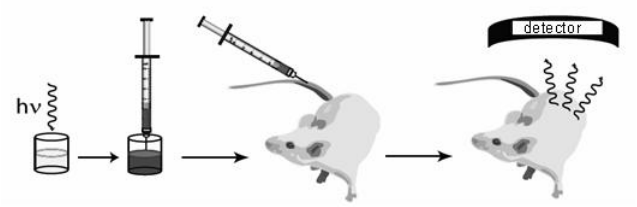

Fig. 10 Bioimaging with PLNP: the principle.

4.2 Influence of coating on the biodistribution of 180 nm PLNP

Biodistribution of 180 nm PLNP with different surface coatings (either amino, carboxy, or PEG) was monitored 30 minutes after systemic injection in mice. Acquired images are shown in Figure 11. For positive amino-PLNP, an important lung retention was observed (Figure 11a). During the first hour, there was little change in this distribution, except a progressive PLNP release from lungs to liver and spleen. Two reasons can explain this biodistribution pattern [Song et al. 1998]. The first one is a nonspecific electrostatic interaction of amino-PLNP with the negative charges displayed by plasmatic membranes of capillary endothelial cells, such as sulfated proteoglycans and glycosylaminoglycans. Another explanation could be provided by aggregation of amino-PLNP with negatively charged blood components, leading to trapping agglomerates of increased size in the narrow lung capillaries. Negative carboxy-PLNP were rapidly cleared from blood flow by liver uptake (Figure 11b). This biodistribution pattern presumably resulted from a rapid opsonisation and an uptake by endothelial and Kupffer cells of the reticuloendothelial system (RES), as is generally observed for nanoparticles or liposomes [Kamps et al. 1997][Krieger et al. 1994]. Neutral PEG-PLNP were able to circulate longer, as assessed by a diffuse signal throughout the mouse body that lasted for the rest of the acquisition time (Figure 11c). However, biodistribution images clearly

show liver accumulation after 60 minutes. When Kupffer cells were saturated by prior administration of anionic liposomes, the neutral PEG-PLNP circulation time increased further (images not shown).

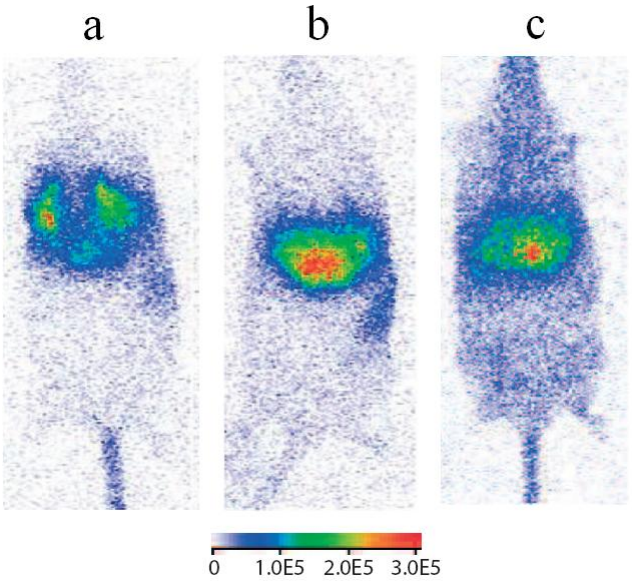

Fig. 11 Biodistribution of PLNP 30 minutes after tail vein injection. a: amino-PLNP. b: carboxy-PLNP. c: PEG-PLNP. [le Masne de Chermont et al. 2007]

4.3 Influence of nanoparticle diameter and PEG chain length on the biodistribution in healthy mice

The biodistribution of PLNP was studied in function of nanoparticle diameter (80, 120 and 180 nm) and PEG chain length (5, 10 and 20 kDa). Relative long-term biodistribution in healthy mice was achieved six hours after systemic injection to validate a potential use of this probe for in vivo applications. Delayed fluorescence from europium ions trapped in the core of the nanoparticles allowed an ex vivo quantitative analysis through tissue homogenates after animal sacrifice. As shown in Figure 12, similarly to several classes of nanoparticles, and regardless of surface coverage, long term PLNP biodistribution occurs predominantly within liver and spleen [Minchin et al. 2010]. Combined uptake in the kidneys and lungs remains below 5 % of the injected dose. The PEG chain length seems to have little influence on the global RES accumulation (combined uptake in liver and spleen), and is only

responsible for a slight change in the liver/spleen ratio (only noticeable for 120 nm PLNP). On the contrary, the nanoparticle core diameter appears to be critical. As shown in Figure 12, decreasing the particle core diameter from 180 nm to 80 nm causes a much lower combined RES uptake of PEG-PLNP from 100 % down to around 35 % of the injected dose [Maldiney et al. 2011].

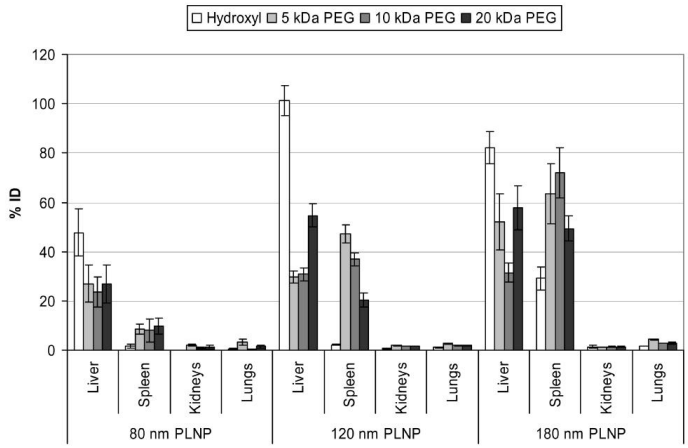

Fig. 12 PLNP tissue distribution 6 hours after systemic injection to healthy mice (n=6). Error bars correspond to standard deviation. [Maldiney et al. 2011]

4.4 Biodistribution of PEG-PLNP in tumor bearing mice

Malignant tumours display both increased angiogenesis and chaotic microenvironment growth, mainly responsible for hypervascularization, leaky vasculature, and poor lymphatic drainage [Maeda et al. 2000]. The pore size in the vasculature ranges from 200 to 600 nm in diameter, leading to an enhanced permeability and retention (EPR) effect [Brannon-Peppas et al. 2004]. It was reported that long-circulating nanoparticles with PEG modifications on their surface were able to conduct passive tumour targeting [Moghimi et al. 2001][Greenwald 2001]. The injection of our 180 nm PEG-PLNP to C57BL/6 mouse bearing an s.c. implanted Lewis lung carcinoma (3LL) tumour in the inguinal region, allowed us to detect the tumour vasculature the first 2 minutes after injection (Figure 13a). However no passive accumulation of our PLNP-PEG could be observed at longer time (Figure 13b). In order to favour a passive accumulation of PEG-PLNP in the tumour area we have recently reported the influence of both the diameter of the PLNP (80, 120 and 180 nm) and the length of the PEG chain (5, 10 and 20 kDa). This study revealed that

after intravenous injection of 80 nm PLNP-PEG$_{10kDa}$ in 3LL tumour bearing mice, 5.9 ± 2.8 % of the injected dose were located within the tumour micro-environment 6 hours after the injection [Maldiney et al. 2011].

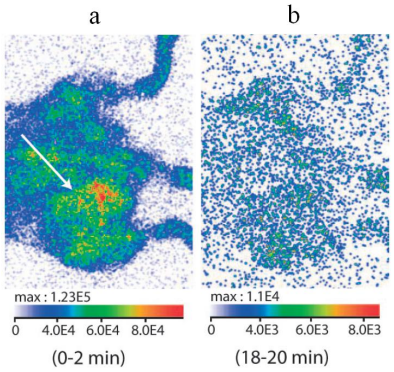

Fig. 13 Images of PLNP-PEG injected to a mouse bearing an s.c. implanted Lewis lung carcinoma (3LL) tumor. a: image obtained 2 minutes after injection. b: image obtained 20 minutes after injection of PLNP. [le Masne de Chermont et al. 2007]

Another way to target tumour vasculature is to use nanoparticles coated with targeting ligands [Richard et al 2008][Byrne et al. 2008][Loomis et al. 2011]. Efforts in our laboratory are actually directed towards surface functionalization of PLNP with ligands able to target receptors of interest.

4.5 PLNP for imaging inflammation in a mouse model of arthritis

Rheumatoid synovium is characterized by hyperplasia of the synovial lining layer and marked infiltration by lymphocytes, macrophages and plasma cells. Locally produced inflammatory mediators and subsequent up-regulation of adhesion molecules within inflammation sites are both pivotal to the development of rheumatoid arthritis [Choy et al. 2001][Tak et al. 1996].
Neoangiogenesis is also a vital component of pannus formation. The early diagnosis of rheumatoid arthritis is made problematic by heterogeneity in its clinical presentation and uncertainty about which patients will respond to treatment. Sensitive and specific imaging methods are required for the detection of early inflammatory changes to the synovium in patients with arthritis and for monitoring response to treatment.
We have evaluated the capacity of carboxy and PEG-PLNP to reveal inflammatory sites in an experimental mouse model of arthritis. The pathology was induced in the DBA/1 mice by immunization with 100 μg of bovine collagen type II at the base of the tail on day 0 and day 21 [Courties et al. 2009]. Thirty days after immunization,

100 μg of PLNP (carboxy or PEG) previously excited with a UV lamp for 5 min were injected in the tail vein. Their biodistribution was then monitored under the photon-counting system (Figure 14).

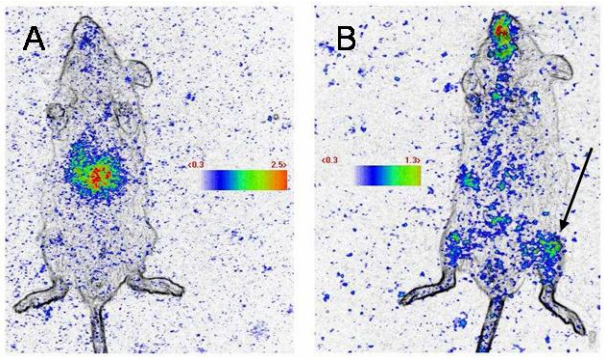

Fig. 14 PLNP for imaging inflammation sites. A: image obtained with carboxy-PLNP 30 minutes after injection. B: image obtained with PEG-PLNP. In both cases $GdCl_3$ was injected before PLNP to increase the circulation time of the nanoparticles. The black arrow indicates the site of inflammation.

As shown in Figure 14-A, carboxy-PLNP were quickly trapped in liver, even in the presence of $GdCl_3$ (generally used to saturate liver macrophages). In contrast, PEGylated PLNP evade liver (Figure 14-B) to accumulate in the hind legs, at sites of inflammation, and in the oral cavity which is a highly vascularized area. Surface and diameter of the PLNP are key elements that we are actually modifying to improve these results.

5 Conclusion

We described the synthesis of several persistent luminescence nanoparticles from silicate host. Among them, $Ca_{0.2}Zn_{0.9}Mg_{0.9}Si_2O_6$ doped with Eu^{2+}, Dy^{3+}, and Mn^{2+} appeared as the most interesting material for bioimaging applications in terms of emission wavelength and intensity of luminescence. We extracted different monodisperse nano-sized distributions (from 80 to 180 nm) and showed that surface functionalization could not only drastically improve their biodistribution in healthy and tumor-bearing mice, but could also allow to monitor inflammation in a mouse model of arthritis. These results are encouraging, and additional works are actually in progress to heighten image analysis of the acquired data by the means of more reliable softwares and computational tools, but also to improve PLNP optical performances, biodegradability and targeting capabilities.

There remain several challenges associated with this innovative technique. First, as luminescence decreases with time, background signal becomes predominant. After approximately one hour, signal from PLNP is not detectable anymore. This first limitation requires to focus on persistent luminescence materials, and to find new compositions with improved optical properties. Then, two-dimensional optical detection raises the problem of photons diffusion, depth-dependent, that blurs biological structures contours and hampers organs distinction. Therefore, we sometimes observe distorted organs (such as liver or spleen) with variable shape and size. To circumvent this last issue, valuable efforts are being made to work on three-dimensional acquisition systems that would permit combined acquisition in several plans, as well as image reconstruction of the organ through highly developed softwares designed to return the corrected shape and size of the organ from acquired data.

References

[Brannon-Peppas et al. 2004] Brannon-Peppas L, Blanchette JO (2004) Nanoparticle and targeted systems for cancer therapy. Adv Drug Deliv Rev 56:1649-1659.

[Brinker et al. 1990] Brinker CJ, Scherer GW, Sol-Gel Science: The physics and the chemistry of sol-gel processing, 1990 (academic London)

[Byrne et al. 2008] Byrne JD, Betancourt T, Brannon-Peppas L (2008) Active targeting schemes for nanoparticle systems in cancer therapeutics. Adv Drug Deliv Rev 60:1615-1626.

[Chen et al. 2005] Chen W, Mahmood U, Weissleder R, Tung C (2005) Arthritis Imaging Using a Near-Infrared Fluorescence Folate-Targeted Probe. Arthritis Res Ther 7: R310-317.

[Choi 2007] Choi HS (2007) Renal Clearance of Quantum Dots. Nat Biotechnol. 25:1165-1170.

[Choy et al. 2001] Choy EH, Panayi GS (2001) Cytokine pathways and joint inflammation in rheumatoid arthritis. N Engl J Med 344:907-916.

[Courties et al. 2009] Courties G, Presumey J, Duroux-Richard I, Jorgensen C, Apparailly F (2009) RNA interference-based gene therapy for successful treatment of rheumatoid arthritis. Expert Opin Biol Ther 9:535-538.

[Greenwald 2001] Greenwald R B (2001) PEG drug: an overview. J Controlled Release 74:159-171.

[Jiang et al. 2003] Jiang L, Chang C, Mao D (2003) Luminescent properties of $CaMgSi_2O_6$ and $Ca_2MgSi_2O_7$ phosphors activated by Eu^{2+}, Dy^{3+} and Nd^{3+}. J Alloys Comp 360:193-197

[Kamps et al. 1997] Kamps JA, Morselt HWM, Swart PJ, Meijer DKF, Scherphof GL (1997) Massive targeting of liposomes, surface-modified with anionized albumins, to hepatic endothelial cells. Proc Natl Acad Sci USA 94:11681-11685.

[Krieger et al. 1994] Krieger M, Herz J (1994) Structures and functions of multiligand lipoprotein receptors: macrophage scavenger receptors and LDL receptor-related protein. Annu Rev Biochem 63:601-637.

[le Masne de Chermont et al. 2007] le Masne de Chermont Q, Chanac C, Seguin J, Pelle F, Matrejean S, Jolivet JP, Gourier D, Bessodes M, Scherman D (2007) Nanoprobes with Near-Infrared Persistent Luminescence for In Vivo Imaging. Proc Natl Acad Sci USA104:9266-9271.

[le Masne de Chermont et al. 2009] le Masne de Chermont Q, Richard C, Seguin J, Chanac C, Bessodes M, Scherman D (2009) Silicates doped with luminescent ions: useful tools for optical imaging applications. Proc of SPIE 7189:71890B/1-71890B/9.

[Li et al. 2004] Li ZF, Ruckenstein E (2004) Water-soluble poly(acrylic acid) grafted luminescent silicon nanoparticles and their use as fluorescent biological staining labels. Nano Lett 4:1463-1467.

[Longmire et al. 2008] Longmire M, Choyke PL, Kobayashi H (2008) Clearance properties of nano-sized particles and molecules as imaging agents: considerations and caveats. Nanomedicine 3:703-717.

[Loomis et al. 2011] Loomis K, McNeeley K, Bellamkonda RV (2011) Nanoparticles with targeting, triggered release, and imaging functionality for cancer applications. Soft Matter 7:839-856.

[Maeda et al. 2000] Maeda H, Wu J, Sawa T, Matsumura Y, Hori K (2000) Tumor vascular permeability and the EPR effect in macromolecular therapeutics: a review. J Controlled Release 65:271-284.

[Maldiney et al. 2011] Maldiney T, Richard C, Seguin J, Wattier N, Bessodes M, Scherman D (2011) Effect of core diameter, surface coating and PEG chain length on the biodistribution of persistent luminescent nanoparticles in mice. ACS Nano 5:854-862

[Medintz et al. 2005] Medintz IL, Uyeda HT, Goldman ER, Mattoussi H (2005) Quantum dot bioconjugates for imaging, labelling and sensing. Nat Mate. 4:435-446.

[Minchin et al. 2010] Minchin RF, Martin DJ (2010) Nanoparticles for molecular imaging - an overview. Endocrinology 151:474-481.

[Moghimi et al. 2001] Moghimi SM, Hunter C, Murray JC (2001) Long-circulating and target-specific nanoparticles: theory to practice. Pharmacol Rev 53:283-318.

[Park et al. 2009] Park JH, Gu L, von Maltzahn G, Ruoslahti E, Bhatia SN, Sailor MJ (2009) Biodegradable luminescent porous silicon nanoparticles for in vivo applications. Nat Mater 8:331-336.

[Resch-Genger et al. 2008] Resch-Genger U, Grabolle M, Cavaliere-Jaricot S, Nitschke R, Nann T (2008) Quantum dots versus organic dyes as fluorescent labels. Nat Methods 5:763-775.

[Richard et al 2008] Richard C, le Masne de Chermont Q, Scherman D (2008) Nanoparticles for imaging and tumor gene delivery. Tumori 94: 264-270.

[Salonen et al. 2007] Salonen J, Kaukonen AM, Hirvonen J, Lehto VP (2007) Mesoporous silicon in drug delivery applications. J Pharm Sci 97:632-653.

[Smith et al. 2008] Smith AM, Duan H, Mohs AM, Nie S (2008) Bioconjugated quantum dots for in vivo molecular and cellular imaging. Adv Drug. Deliver Rev 60:1226-1240.

[Song et al. 1998] Song YK, Liu F, Liu (1998) Enhanced gene expression in mouse lung by prolonging the retention time of intravenously injected plasmid DNA. Gene Ther 5:1531-1537.

[Tak et al. 1996] Tak PP, Taylor PC, Breedveld FC Smeets TJM, Daha MR, Kluin PM, Meinders AE, Maini RN (1996) Decrease in cellularity and expression of adhesion molecules by anti-tumor necrosis factor alpha monoclonal antibody treatment in patients with rheumatoid arthritis. Arthritis Rheum 39:1077-81.

[Wang et al. 2003] Wang XJ, Jia D, Yen WM (2003) Mn^{2+} activated green, yellow, and red long persistent phosphors. J Lumin. 103:34-37

[Weissleder et al. 2008] Weissleder R, Pittet MJ (2008) Imaging in the era of molecular oncology. Nature 452:580-589.